XLIII CILAMCE
21–25, November, 2022
FOZ DO IGUAÇU – PR – BRAZIL

A Multiscale Model to Simulate the Bone Remodeling Process

José E. Gubaua[1], Gabriela W.O. Dicati[2], Emilio G.F. Mercuri[3], Jucélio T. Pereira[4]

[1]*Laboratory of Computational Solid Mechanics, Postgraduate Program in Mechanical Engineering, Federal University of Paraná, Curitiba, Brazil*
gubaua@ufpr.br
[2]*Laboratory of Computational Solid Mechanics, Postgraduate Program in Mechanical Engineering, Federal University of Paraná, Curitiba, Brazil*
gabioening@gmail.com
[3]*Dept. Environmental Engineering, Federal University of Paraná, Curitiba, Brazil*
emilio@ufpr.br
[4]*Dept. Mechanical Engineering, Federal University of Paraná, Curitiba, Brazil*
Laboratory of Computational Solid Mechanics, Postgraduate Program in Mechanical Engineering, Federal University of Paraná, Curitiba, Brazil
Jucelio.tomas@ufpr.br

Abstract. Bone tissue is a living material under constant activity. Bone response to an external stimulus application causes renewal of its local properties by the bone remodeling process. The synchronized activities of three bone cell lineages are related to the process. The osteoblast lineage is responsible for bone formation, while the osteoclasts are responsible for the resorption process. Finally, the osteocytes cells provide mechanosensitivity to the bone tissue. An important factor for controlling the cell activity is the OPG-RANKL-RANKL pathway. Another characteristic of the bone tissue is its multiscale behavior. The behavior at the microscale influences the properties at the macroscale. In this sense, this study aims to develop a model for simulating the bone remodeling process. This model considers mechanical, chemical, and biological variables, and the bone multiscale. We use the finite element method to analyze the remodeling process by using Abaqus and Matlab software. The biological model considers the interactions between osteoblasts and osteoclasts. Also, the model considers the control performed by the OPG-RANKL-RANKL pathway. We determine the mechanical stimulus at the microscale using a representative volume element (RVE). This stimulus interacts with chemical factors. This interaction controls the bone cell evolution that changes the RVE's volume fractions. Thus, the volume fractions evolution influences the mechanical properties at macroscale (density and elastic modulus). The BR model allowed characterizing the structural morphology of a human femur. We observed its main characteristics.

Keywords: cell activity, bone adaptation, numerical approach, bone tissue, Abaqus.

1 Introduction

Bone tissue is the primary material that composes the human skeleton. This material presents extreme complexity, significant heterogeneity, porosity, and anisotropy. Also, the bone changes its internal structure and adapts to the loads applied [1]. Bone remodeling (BR) performs the process of evolving bone tissue properties. BR performs the replacement of damaged tissue with a new and healthy one. Specialized cells promote bone resorption (osteoclasts) and formation (osteoblasts) [2].

There are several approaches to describe the BR. The first approach is phenomenological. This approach describes the bone response to the load case applied [3-5]. A second approach is biological. Here, biochemical factors and bone cells describe bone tissue resorption and formation. Usually, a system of differential equations simulated the behavior of each cell population over time [2,6]. Thus, it is possible to validate the model by comparing numerical and experimental results. A third approach is mechanobiological and it uses the concepts

presented before. The mechanobiological approach allows simulating the biological behavior of bone tissue [7,8]. Both phenomenological and mechanobiological approaches use a stimulus determined by mechanical variables associated with macroscale. Some mechanobiological models use the concepts of continuum micromechanics [9,10]. Bone tissue is a material with a well-contextualized hierarchy. Thus, the bone's macroscopy behavior is directly related to the response in the microscopy phase. Researchers developed the multiscale theories to describe the responses given by microscopic structures. At the microscopic scale, there are heterogeneities of different geometries, dimensions, materials, empty or not, which affect the properties at the macroscale [11,12]. Thus, the multiscale approach allows determine the microstructural responses by considering the material's characteristics at this phase.

Thus, we used a micromechanical model with mechanobiological interaction to simulate the BR [5,13]. We verified whether the model predicts the cortical formation from a femur with an initial homogeneous density distribution. Here, we considered the micromechanical stimulus as the leading variable of the process. Thus, evolution of cell populations responsible for bone formation and resorption is simulated. Also, we implemented an approach for describing the micromechanical stimulus following the macroscopic approach presented by Jacobs et al [4].

2 Methodology

The BR model considers the continuum micromechanics for determining the mechanical stimulus. This variable leads the biological interaction. We described the concepts used for implementing the BR model below.

2.1 Biological model

We used the same biological approach used by Gubaua et al. [5] and Mercuri et al. [13]. The model considers the populations of responsive (R) and active (B) osteoblasts and active (C) osteoclasts. The mechanical stimulus and RANK-RANKL-OPG mediate the biological interactions. We used 4 differential equations over the time (t) for describing the cell populations and bone volume (BV). This system is giving as

$$\begin{aligned} \frac{dR}{dt} - D_R\pi_C - P_R\, R\, \Pi_W + \frac{D_B R}{\pi_C} = 0, \\ \frac{dB}{dt} - \frac{D_B R}{\pi_C} + k_B B = 0, \\ \frac{dC}{dt} - D_C\, \pi_L + D_A \pi_C C = 0, \\ \frac{dBV}{dt} - k_{form} B + k_{res} C = 0. \end{aligned} \tag{1}$$

We describe the RANKL production (π_L) as

$$\pi_L = \frac{k_3}{k_4} \frac{K_L^P \pi_P B}{1+\frac{k_3}{k_4} k_{RANK} + \frac{k_1}{k_2}\frac{K_0^P P}{k_0}} \left(1 + \frac{I_L}{r_L} + P_{RANKL_W}\right). \tag{2}$$

The micromechanical stimulus (w) regulates the RANKL production by following

$$P_{RANKL_W} = \begin{cases} \kappa\left(1 - \frac{w}{w_{lower}}\right) & if \quad w \le w_{lower}, \\ 0 & if \quad w > w_{lower}. \end{cases} \tag{3}$$

The function that governs the PTH (π_P) follows

$$\pi_P = \frac{S_P}{k_P}\frac{k_5}{k_6} \tag{4}$$

Finally the level of mechanical microstimulus (w) controls the R population as

$$\Pi_w = \begin{cases} \Pi_{w_{equi}}\left[1 + \lambda\left(\frac{w}{w_{upper}} - 1\right)\right] & if \quad w \ge w_{upper} \\ \Pi_{w_{equi}} & if \quad w < w_{upper}, \end{cases} \tag{5}$$

Table 1 presents the description of the parameters used to describe the biological process.

Table 1. Parameters used to describe the biological model

Parameter	Unit	Value	Description [Reference]
D_A	day^{-1}	2.660768	Rate of osteoclast apoptosis caused by $TGF-\beta$ [2]
d_B	day^{-1}	0.70	Differentiation rate of responding osteoblasts [13]
d_C	pM day^{-1}	2.1×10^{-3}	Differentiation rate of osteoclasts precursors [2]
D_R	pM day^{-1}	0.0070744	Differentiation rate of osteoblast progenitors [13]
f_0	-	0.05	Fixed proportion [2]
K	pM	1.0×10^{1}	Fixed concentration of RANK [2]
k_1	pM day^{-1}	1.0×10^{-2}	Binding rate of OPG-RANKL [2]
k_2	day^{-1}	1.0×10^{1}	Unbinding rate of OPG-RANKL [2]
k_3	pM day^{-1}	5.8×10^{-4}	Binding rate of RANK-RANKL [2]
k_4	day^{-1}	1.7×10^{-2}	Unbinding rate of RANK-RANKL [2]
k_5	pM day^{-1}	2.0×10^{-2}	Binding rate of PTH with its receptor [2]
k_6	day^{-1}	3.0	Unbinding rate between PTH and its receptor [2]
k_B	day^{-1}	0.7184	Rate of active osteoblast elimination [2]
K_L^P	pM cell^{-1}	3.0×10^{6}	Maximum quantity of RANKL on the cell's surface [2]
k_0	day^{-1}	0.35	Rate of OPG elimination [2]
K_0^P	pM $\text{day}^{-1}\text{cell}^{-1}$	2.0×10^{5}	Minimum production rate of OPG per cell [2]
k_P	day^{-1}	86.0	Rate of PTH elimination [2]
r_L	pMday^{-1}	1.0×10^{3}	Rate of RANKL production and elimination [2]
S_P	pM day^{-1}	2.5×10^{2}	Rate of systemic PTH synthesis [2]
k_{res}	cell^{-1}	2.72×10^{1}	Relative rate of bone resorption per osteoclast [2]
k_{form}	cell^{-1}	3.409×10^{1}	Rate of bone formation per osteoblast [2]
P_R	pM day^{-1}	0.1694	Proliferation rate of responsive osteoblasts [2]
λ	pM day^{-1}	$1.2 \quad if \quad w \geq w_{\text{upper}}$ $0 \quad if \quad w < w_{\text{upper}}$	Adjustment parameter [13]
$\Pi_{w_{equi}}$	-	1.2	Equilibrium value of mechanoregularoty function [13]
κ	pM day^{-1}	$500 \quad if \quad w \leq w_{\text{lower}}$ $0 \quad if \quad w > w_{\text{lower}}$	Parameter to correct the production of RANKL by the mechanical stimulus [13]
w^*	MPa	150.0	Equilibrium mechanical stimulus
w_{upper}	MPa	$w^* + 0.1250w^* = 168.75$	Upper limit of lazy zone
w_{lower}	MPa	$w^* - 0.1250w^* = 131.25$	Lowe limit of lazy zone
n		3000	Number of cycles
m		4.0	Empirical constant [4]
ν_{HA}		0.27	Poisson ratio of hydroxyapatite [14]

2.2 Continuum micromechanics

We used three main concepts for characterizing the micromechanics. The first concept is representation. The representation is the identification and mechanical characterization of each phase of the RVE. In this study, we used the TVE composed of a mineralized phase (bone matrix) and a vascular phase. They received the indices bm and vas. The second concept is localization. The localization establishes the relation between the states of strain at the boundary and interstitial (homogeneous) phases of the RVE. Finally, the third concept is homogenization. The homogenization allows the determination of the homogeneous macroscale properties. For this, we use the properties, volume fraction, and morphology of each phase of the RVE.

We determine the homogenization of the stiffness at microscale (C_B^{hom}) for bone tissue as [9]

$$C_B^{hom} = \sum_r f_r C_r : A_r^{est}. \tag{6}$$

In this equation, f_r is the volume fraction of the phase r, C_r is the 4th-order constitutive tensor order at microscale associates to the phase f. Finally, A_r^{est} is the concentation tensor of the phase.

We determine the concentration tensor by using the classical matrix-inclusion problem, proposed by Eshelby [15], by means of Mori-Tanaka scheme [16] as [14]

$$A_r^{est} = \left[I + P_r^0\left(C_r^{(\mu)} - C_0^{\mu}\right)\right]^{-1} : \left\{\sum_s f_s\left[I + P_s^0\left(C_s^{(\mu)} - C_0^{\mu}\right)\right]^{-1}\right\}^{-1}, \tag{7}$$

where I is the fourth-order unit tensor and P_r^0 is the fourth-order Hill tensor related to the format of the phase r. We considered it as an isotropic inclusion in the matrix with stiffness C_0^{μ}.

The evolution of the biological model describes the temporal behavior of biological variables and allows us

to determine the volume fractions. We determine the stiffness tensor for each phase following Sheiner et al. [9]. The macroscale density (ρ) has a linear relationship with BV [13].

2.3 Mechanical stimulus at the microscale

We used the continuum stress at the macroscale (called apparent stress) for determining the mechanical stimulus. The concepts of continuum mechanics and micromechanics describe the macroscale and microscale. Also, microscale's phases, which compose the REV, are isotropic. We determine the apparent stress by using the strain energy density (U_{bm}^{μ}) and the respective Elastic modulus (E_{bm}^{μ}) at microscale ($\bar{\sigma}_{bm}^{\mu}$) as

$$\bar{\sigma}_{bm}^{\mu} = \sqrt{2\, E_{bm}^{\mu}\, U_{bm}^{\mu}}\ . \tag{8}$$

For determining (E_{bm}^{μ}), we considered the microscale phase with elastic, linear, and isotropic behaviors. The generalized Hooke law describes the phase's behavior. In this sense and by using the component C_{1111} of the microscale stiffness tensor C_{bm}^{μ}, we obtain the elastic modulus E_{bm}^{μ} as

$$C_{1111} = \frac{E_{bm}^{\mu}}{1+\nu_{HA}}\left[\frac{1-\nu_{HA}}{1-2\nu_{HA}}\right]\ . \tag{9}$$

In this equation, ν_{HA} is the Poisson ratio of hydroxyapatite (constituent of bone matrix). We use $\overline{\sigma}_{bm}^{\mu}$ to determine the effective stress ($\overline{\sigma}_{t_{bm}}^{\mu}$) following

$$\bar{\sigma}_{r}^{\mu} = \left(\frac{f_{bm}}{f_{total}}\right)^2 \bar{\sigma}_{t_{bm}}^{\mu}\ , \tag{10}$$

where f_{total} is the total volume fraction of the RVE. One can note the total volume fraction is equal to 1. In this way, the mechanical stimulus at the microscale only depends on the fraction volume of the bone matrix and the number of cycles of each load condition (n_i). Thus, we determine the mechanical stimulus w at the microscale following

$$w = \left(\sum n_i \bar{\sigma}_{t_{bm_i}}^{(\mu)m}\right)^{1/m}\ . \tag{11}$$

Thus, both the evolution of cell populations and the updating of the density (at the macroscale) depend on all load conditions considered.

2.4 Elasticity at the macroscale

The elastic modulus (E) of bone tissue depends on the bone apparent density (ρ) and follows [4]

$$E(\rho)[MPa] = 3790\ \rho^3\ . \tag{12}$$

We kept the Poisson ratio (ν) constant along the simulation with a value equal to 0.30 [4].

2.5 Geometric and finite element models of the human femur

The geometry used [17] represents the proximal part of a human femur (Fig. 1a). We imported this geometry to the software Abaqus to develop the finite element model. The linear tetrahedral finite element C3D4 discretizes the geometry. A total of 86,320 elements and 17,164 nodes composes the mesh used (Fig. 1b). We used standard forces that correspond to a step of a gait cycle that consists of six loads. Three of these loads correspond to compression on the femoral head. The remaining three describe the muscle tension on the greater trochanter. Three instants represent the step of a gait cycle: (i) when the foot touches the floor, (ii) flection, and (iii) extension of the lower limb. Beaupré, Orr, and Carter [18] provide the intensities of the laods. We followed Greenwald and Haynes [19] and Bagge [20] to determine the regions for the loads on the femoral head and greater trochanter. Finally, we determine the orientation of the loads on the greater trochanter based on Bagge [20]. Table 2 presents the intensity and orientation of the load conditions used. One can visualize this load condition in Dicati et al. [21].

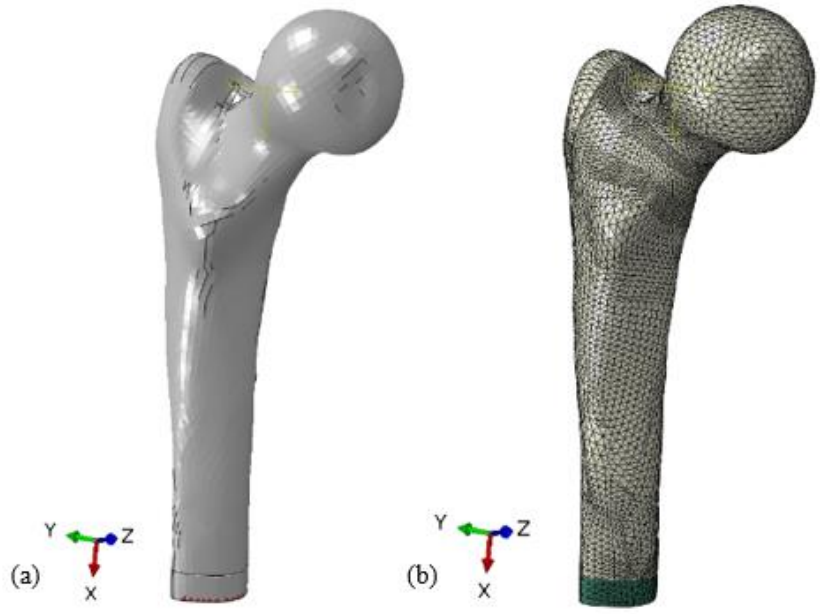

Figure 1. Femur's geometry (a) used in this study and (b) finite element mesh.

Table 2. Intensity and orientation of the loads applied

Load	Intensity (N)	Orientation[1] (grades)
Compression-1	1158	Pressure (normal to surface)
Compression-2	2317	Pressure (normal to surface)
Compression-3	1548	Pressure (normal to surface)
Traction-1	351	27,53; 29,3; 59,65
Traction-2	703	-5,933; 2,848; 39,29
Traction-3	468	23,28; -27,93; 62,17

[1] Coordinate system: x-axis represents the lateral-medial direction, y-axis the anterior-posterior direction, and z-axis for lower-upper direction

We applied homogeneous Dirichlet boundary conditions to balance the load condition. They were applied to a small solid inserted into the medial part of the femoral diaphysis. This solid has elastic, linear, and isotropic behavior. We used it to prevent stress concentrations in the femoral model [5,21,22].

2.6 Flowchart

The implementation of the BR model used in this study follows the flowchart presented in Fig. 2. We implemented a computational structure by using Abaqus and Matlab software packages. The software Abaqus determines the stress distribution. For this, we implemented a subroutine UMAT. This contains the equations to predict the bone behavior. The software Matlab reads the stress distribution to perform the stress smoothing. The cubic relation of elastic modulus and bone density allows the formation of a numerical instability called checkerboard. This instability generates an increase in stiffness in regions where the density is close to 1,0 g/cc [22]. Thus, we perform the stress smoothing by simple nodal average to mitigate this problem [22]. As indicated by Gubaua et al. [22], the smoothing process applied on the density solves the checkerboard problem, but it acts as a kind of filter for the density field. This inhibits the correct femoral characterization. The BR simulation starts with a homogeneous distribution of properties described by the roots of the Eq. (1). The values of R, B, C, and BV were equal to $7.7341e^{-4}$, $7.2848e^{-4}$, $9.1262e^{-4}$ pM, and 0.50. These properties describe both cortical and trabecular bones.

We used the smoothed stress to determine the stress at the microscale. Thus, the micromechanical stimulus (w) can be determined. It is used in the equation that describes the interaction of the cells that participates in the

BR process. We used the fourth-order Runge-Kutta method for solving Eq. (1). Finally, the macroscale properties are updated. This process occurs until the number of iterations (1,000) is reached.

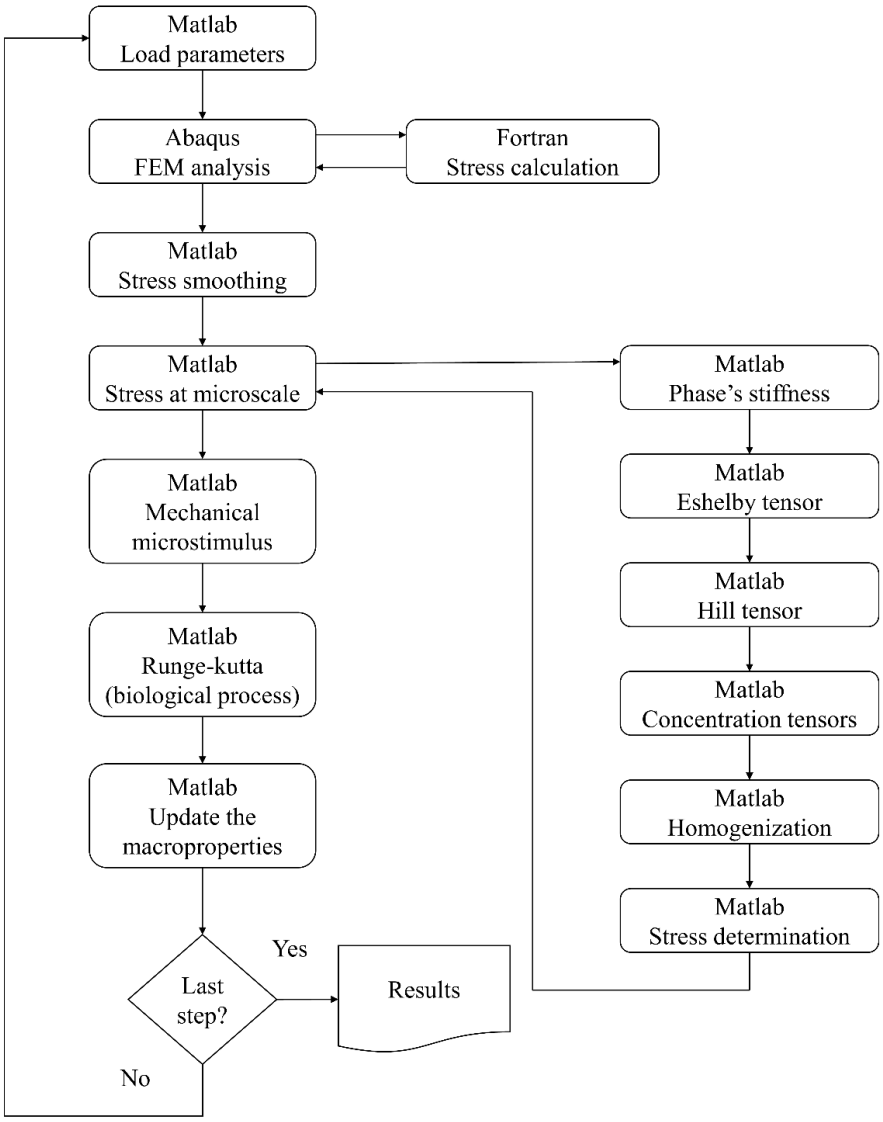

Figure 2. Flowchart of the BR process.

3 Results and discussions

The simulation of the microscale BR process (Fig. 3) allowed the femoral morphology characterization (Fig. 3e). One can note the main aspects of the femur. We can cite the deposition of cortical bone surrounding the diaphysis, the formation of the medullar cavity inside the diaphysis, and the trabecular density distribution over the proximal region. However, the distribution presents a large cortical thickness than when compared with clinical data. This considerable cortical happens due to the smoothing stress process for mitigating the checkerboard [22]. Without the checkerboard, there is a structure less stiff. It needs to form more bone to resist the same stimuli that the distribution with the checkerboard resists. One solution is to increase the value of the reference mechanical stimulus (w^*).

Biological variables received initial constant values (equilibrium condition of eq. (1)). The micromechanical stimulus (w) deviates the values of cell populations, which leads the bone formation and resorption. The tendency is after the deviation, the functions return to the equilibrium condition. But, with a heterogeneous BV distribution (Fig. 3e). Although the cell population present more elevated levels at regions surrounding the femoral diaphysis,

one can visualize this behavior on Fig. 3d. This region presents high-levels of mechanical stimulus due to the Dirichlet boundary conditions. The cell populations are not effective to return to the equilibrium condition due to the lazy zone (eqs. (3) and (5)). Another important factor is the different powers used in eqs. (11) and (12) [23]. Different values lead to a condition of numerical instability of the BR model.

Although the formulation considered biological variables, the tissue behavior was closer to a BR phenomenological approach. The main aspect visualized in the simulation was the femoral characterization (Fig. 3e) obtained from an initial homogeneous BV distribution. Other aspects of the BR process need to be inserted into the model's formulation to become it a more representative tool of the actual process. The first aspect is to use different parameters to describe the trabecular and cortical bone behaviors. The second aspect is to adopt a process for damage accumulation and repair. The microdamage interrupts the communication between osteocytes. Then, the osteoclasts concentration increases at the bone site. So, there is more bone resorption. Another factor is to consider bone mineralization, which is a fundamental aspect of simulating the bone stiffness evolution over time. Since the bone can store important mineral salts such as calcium. Those aspects would turn the model into a more realistic tool. This is also valid for de biological time of the BR process.

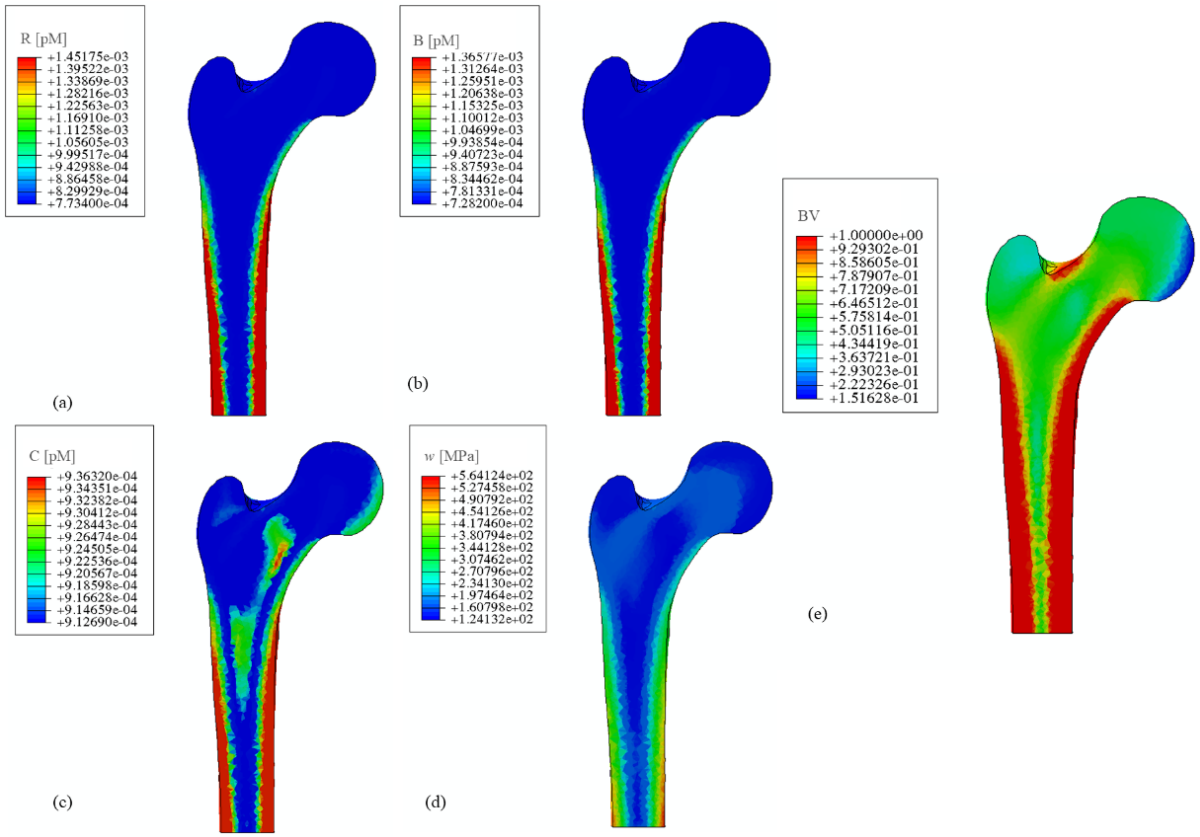

Figure 3. Cells, BV, and micromechanical stimulus distributions after 1,000 iterations, being distributions of (a) R, (b) B, (c) C, (d) w, and (e) BV.

4 Conclusions

This study combined chemical, biological, and mechanical variables into a microscale approach to simulate the BR. Also, we implemented an approach to describe the micromechanical stimulus. The BR model allowed characterizing the structural morphology of a human femur. We observed its main characteristics.

Computational models that use different variables of the BR can become useful tools for developing drug therapies. This tool could allow knowing what happens with a determined aspect of the bone when it interacts with drugs. Also, we could see what this interaction can cause to macroscale over time.

Acknowledgements. This study was financed in part by the Coordenação de Aperfeiçoamento de Pessoal de Nível Superior - Brasil (CAPES) - Finance Code 001.

Authorship statement. The authors hereby confirm that they are the sole liable persons responsible for the authorship of this work, and that all material that has been herein included as part of the present paper is either the property (and authorship) of the authors, or has the permission of the owners to be included here.

References

[1] J. M. García, M. Doblaré and J. Cegoñino, "Bone remodeling simulation: A tool for implant design". *Computational Materials Science*, vol. 25, n. 1, pp. 100-114, 2002.
[2] V. Lemaire, F. L. Tobin, L. D. Greller, C. R. Cho and L. J. Suva," Modeling the interactions between osteoblast and osteoclast activities in bone remodeling". *Journal of Theoretical Biology*, vol. 229, n. 3, pp. 293-309, 2004.
[3] M. Doblaré and J. M. García, "Application of an anisotropic bone-remodeling model based on a damage-repair theory to the analysis of the analysis of the proximal femur before and after total hip replacement**"**. *Journal of Biomechanics*, vol. 34, pp. 1157–1170, 2001.
[4] C. R. Jacobs, M. E. Levenston, G. S. Beaupré, J. C. Simo and D. R. Carter, "Numerical instabilities in bone remodeling simulations: The advantages of a node-based finite element approach". *Journal of Biomechanics*, vol. 28, n. 4, pp. 449-459, 1995.
[5] J. E. Gubaua, G. W. O. Dicati, E. Mercuri and J. T. Pereira, "Simulation of bone remodeling around a femoral prosthesis using a model that accounts for biological and mechanical interactions". *Medical Engineering and Physics*, vol. 84, pp. 126-135, 2020. DOI: 10.1016/j.medengphy.2020.08.004
[6] P. Pivonka, J. Zimak, D. W. Smith, B. S. Gardiner, C. R. Dunstan, N. A. Sims, T. J. Martin and G. R. Mundy, "Model structure and control of bone remodeling: A theoretical study". *Bone*, vol. 43, n. 2, pp. 249-263, 2008.
[7] T. Rüberg, J. M. García-Aznar and M. Doblaré, "A bone remodelling model coupling microdamage growth and repair by 3D BMU-activity". *Biomechanics and Modeling in Mechanobiology*, vol. 4, n. 2-3, pp. 147–167, 2005.
[8] M. Ashrafi, J. E. Gubaua, J. T. Pereira, F. Gahlichi and M. Doblaré, "A mechano-chemo-biological model for bone remodeling with a new mechano-transduction approach". *Biomechanics and Modeling in Mechanobiology*, pp. 1-25, 2020. DOI: 10.1007/s10237-020-01353-0.
[9] S. Scheiner, P. Pivonka and C. Hellmich, "Coupling systems biology with multiscale mechanics, for computer simulations of bone remodeling. *Computer Methods in Applied Mechanics and Engineering*, vol. 254, pp. 181-196, 2013
[10] M. Bahia, M. Henke, E. Mercuri and M. Pinheiro, "A bone remodeling model governed by cellular micromechanics and physiologically based pharmacokinetics", *Journal of the Mechanical Behavior of Biomedical Materials*, vol. 104, pp. 103657, 2020.
[11] E.G.F. Mercuri. Modelagem Multiescala de Tecidos Mineralizados considerando a Micromecânica da Dinâmica Celular. PhD Thesis, Federal University of Paraná, 2013.
[12] P.V.Q. Andrade. Estudo Do Comportamento Mecânico De Microestruturas De Materiais Compósitos Com Matriz Metálica. Dissertation, Federal University of Goiás, 2017
[13] E. Mercuri, A. Daniel, M. Hecke and L. Carvalho. "Influence of different mechanical stimuli in a multi-scale mechanobiological isotropic model for bone remodeling". *Medical Engineering and Physics*, vol. 38, pp. 904-910, 2016.
[14] C. Hellmich, F. J. Ulm, and L. Dormieux, "Can the diverse elastic properties of trabecular and cortical bone be attributed to only a few tissue-independent phase properties and their interactions? Arguments from a multiscale approach", *Biomechanics and Modeling in Mechanobiology*, vol. 2(4), pp. 219-238, 2004
[15] J. D. Eshelby, "The determination of the elastic field of an ellipsoidal inclusion, and related problems", *Proceedings of the Royal Society of London. Series A. Mathematical and Physical Sciences*, v. 254 (1226, pp. 376-396, 1957.
[16] T. Mori and K. Tanaka, "Average stress in matrix and average elastic energy of materials with misfitting inclusions", *Acta Metallurgica*, vol. 21 (5), pp. 571-574, 1973.
[17] GrabCad. Human femur, https://www.grabcad.com/library/femur-1 ; 2012 [accessed 25 November 2016].
[18] G. S. Beaupre, T. E. Orr and D. R. Carter. "An approach for time-dependent bone modeling and remodeling—application: A preliminary remodeling simulation". *Journal of Orthopaedic Research*, pp. 662-670, 1990.
[19] A. S. Greenwald and D. W. Haynes, "Weight-bearing areas in the human hip joint", *The Journal of Bone and Joint Surgery*, vol. 54, pp. 157-163, 1972
[20] M. Bagge, "A model of bone adaptation as an optimization process", *Journal of Biomechanics*, vol. 33, pp. 1349-1357, 2000
[21] G. W. O. Dicati, J. E. Gubaua and J. T. Pereira, "Optimum parameters for each subject in bone remodeling models: A new methodology using surrogate and clinical data", *European Journal of Mechanics / A Solids*, vol. 91, pp. 104409, 2022.
[22] J. E. Gubaua, G. W. O. Dicati, J. Silva, J. L. do Vale and J. T. Pereira. "Techniques for mitigating the checkerboard formation: application in bone remodeling simulations", *Medical Engineering and Physics*, vol. 99, pp. 103739, 2022.
[23] G. W. O. Dicati, J. E. Gubaua and J. T. Pereira, "Analysis of the uniqueness and stability of solutions to problems regarding the bone-remodeling process", *Medical Engineering and Physics*, vol. 85, pp. 113-122, 2020.